Stem Cell Reports
Article

ISSCR

OPEN ACCESS

Human retinal organoids with an *OPA1* mutation are defective in retinal ganglion cell differentiation and function

Qiannan Lei,[1] Kangjian Xiang,[1] Lin Cheng,[1,3] and Mengqing Xiang[1,2,*]

[1]State Key Laboratory of Ophthalmology, Zhongshan Ophthalmic Center, Sun Yat-sen University, Guangdong Provincial Key Laboratory of Ophthalmology and Visual Science, Guangzhou 510060, China

[2]Guangdong Provincial Key Laboratory of Brain Function and Disease, Zhongshan School of Medicine, Sun Yat-sen University, Guangzhou 510080, China

[3]Present address: Department of Ophthalmology and Visual Sciences, University of Iowa Carver College of Medicine, Iowa City, IA, USA

*Correspondence: xiangmq3@mail.sysu.edu.cn

https://doi.org/10.1016/j.stemcr.2023.11.004

SUMMARY

Autosomal dominant optic atrophy (ADOA), mostly caused by heterozygous *OPA1* mutations and characterized by retinal ganglion cell (RGC) loss and optic nerve degeneration, is one of the most common types of inherited optic neuropathies. Previous work using a two-dimensional (2D) differentiation model of induced pluripotent stem cells (iPSCs) has investigated ADOA pathogenesis but failed to agree on the effect of *OPA1* mutations on RGC differentiation. Here, we use 3D retinal organoids capable of mimicking *in vivo* retinal development to resolve the issue. We generated isogenic iPSCs carrying the hotspot *OPA1* c.2708_2711delTTAG mutation and found that the mutant variant caused defective initial and terminal differentiation and abnormal electrophysiological properties of organoid-derived RGCs. Moreover, this variant inhibits progenitor proliferation and results in mitochondrial dysfunction. These data demonstrate that retinal organoids coupled with gene editing serve as a powerful tool to definitively identify disease-related phenotypes and provide valuable resources to further investigate ADOA pathogenesis and screen for ADOA therapeutics.

INTRODUCTION

Autosomal dominant optic atrophy (ADOA) is one of the most common types of inherited optic neuropathies, with prevalence ranging from 1:50,000 to 1:12,000 (Kivlin et al., 1983; Kjer et al., 1996). The main clinical manifestations are moderate to severe visual acuity loss, atrophy of the optic nerve of bilateral eyes, central or paracentric scotomas, and optic disc pallor caused by the loss of retinal ganglion cells (RGCs) with degeneration of the optic nerve. Approximately 60%–70% of all genetically confirmed cases of ADOA have been associated with heterozygous mutations in the *OPA1* gene located on chromosome 3q28-q29, which encodes a dynamin-related mitochondrial guanosine triphosphatase (GTPase) anchored to the inner mitochondrial membrane (Ham et al., 2019; Yu-Wai-Man and Chinnery, 2013). The OPA1 protein contains a transmembrane domain, a GTPase domain, a dynamin domain, and a GTPase effector domain/C-terminal coiled-coil domain (Figure S1A). Most of the *OPA1* mutations reported are substitution, missense, and deletion mutations. Among them, the small fragment deletion mutation c.2708_2711delTTAG located in exon 27 is a hotspot mutation (Figure S1) (Delettre et al., 2001; Weisschuh et al., 2021; Yu-Wai-Man et al., 2010).

The GTPase protein encoded by *OPA1* plays a role in promoting mitochondrial inner membrane fusion and is involved in mitochondrial network organization and cristae remodeling (Alavi and Fuhrmann, 2013; Cipolat et al., 2004). In addition, it is involved in the oxidative phosphorylation process (Alavi and Fuhrmann, 2013; Lodi et al., 2004; Zanna et al., 2008), maintains the respiratory chain and membrane potential (Olichon et al., 2003), and regulates mitochondrial homeostasis via the maintenance of mtDNA integrity. Decreased expression of OPA1 significantly affects mtDNA copy number and distribution throughout the mitochondrial network (Del Dotto et al., 2017; Yang et al., 2020).

OPA1 gene mutations lead to changes in OPA1 protein structure or level, which in turn result in mitochondrial structure damage, optic nerve degeneration, and RGC loss (Alavi and Fuhrmann, 2013; Heiduschka et al., 2010; Yu-Wai-Man et al., 2011). Advances in *in vitro* disease modeling have improved our ability to generate physiologically relevant ADOA models to further understand *OPA1* disease variants. The retinal organoid is a three-dimensional (3D) optic cup in culture that remarkably resembles the embryonic vertebrate eye structure (Eiraku et al., 2011; Nakano et al., 2012). Directed differentiation of human induced pluripotent stem cells (iPSCs) into 3D retinal organoids enables modeling of retinopathy in patient-specific genetic backgrounds (Kruczek and Swaroop, 2020; Parfitt et al., 2016) and also provides a basis for gene correction (Deng et al., 2018). Therefore, organoid technology that combines iPSC technology and gene editing offers a unique research and treatment option that has brought us closer to personalized medicine (Sun and Ding, 2017).

In previous reports, fibroblasts and stem cells were used to study the pathogenesis of *OPA1* mutations (Caglayan et al., 2020; Del Dotto et al., 2017; Olichon et al., 2007; Zanna et al., 2008). However, the mitochondrial content and distribution in different cells are inconsistent, so it is

necessary to study the changes in RGCs, the primary cell type affected by ADOA. More recently, ADOA has been modeled *in vitro* by 2D differentiation using iPSCs carrying haploinsufficient *OPA1* mutations, which were derived from patients or created by gene editing (Chen et al., 2016; Sladen et al., 2022). Severe RGC differentiation defects were observed in iPSCs harboring an *OPA1* mutation in one case (Chen et al., 2016), but no such effect was seen in another (Sladen et al., 2022). Therefore, to resolve such discrepancy and clarify the role of OPA1 in RGC differentiation, in this work, we took advantage of 3D retinal organoids coupled with gene editing to demonstrate that a mutant *OPA1* variant impaired RGC differentiation, causing abnormalities in RGC physiological properties.

RESULTS

Generation of human iPSCs carrying a frequent *OPA1* mutant variant

The c.2708_2711delTTAG mutant variant in *OPA1* exon 27 is one of the most common *OPA1* variants in ADOA, resulting in a premature termination codon that leads to the nonsense-mediated decay (NMD) of *OPA1* mRNA (Brogna and Wen, 2009) and truncation of the protein C terminus (Figure S1). We thus decided to generate iPSCs harboring a heterozygous c.2708_2711delTTAG allele to induce retinal organoids for studying pathogenesis caused by this variant.

For the convenience of identifying and enriching RGCs in retinal organoids, we modified the POU domain transcription factor gene *BRN3B/POU4F2*, which we have demonstrated to be a specific RGC marker (Gan et al., 1996; Xiang et al., 1993). In the UiPSC-001 human iPSC line, which we induced previously from urine cells of a normal person (Cheng et al., 2017), we performed CRISPR-Cas9 gene editing to tether the EGFP reporter gene to the *BRN3B* open reading frame through a P2A self-cleaving peptide sequence (Figure 1A). In this GFP-tagged normal iPSC line, a second gene edit was followed to remove the four nucleotide bases (TTAG) in exon 27 of *OPA1* to generate a mutant iPSC line carrying a heterozygous c.2708_2711delTTAG allele (Figure 1B). Genomic DNA sequencing confirmed the success of this gene edit and heterozygosity of the c.2708_2711delTTAG variant in mutant iPSCs (Figure 1C). By contrast, deep sequencing of the top 10 predicted off-target sites for each of the 3 used single-guide RNAs (sgRNAs) demonstrated no evidence of off-target gene editing, indicating the target specificity of the sgRNAs (Figures S2 and S3).

Immunofluorescent staining showed that both normal and mutant iPSCs had high levels of expression of the pluripotency marker proteins NANOG, OCT4, SOX2, and SSEA4 (Figure S4A), indicating that the c.2708_2711delTTAG variant has no effect on iPSC pluripotency. Moreover, the mutant iPSCs maintained normal karyotype (Figure S4B). To assess whether the c.2708_2711delTTAG variant causes NMD, we carried out a qRT-PCR assay and the result showed that the *OPA1* mRNA level in mutant iPSCs was reduced to approximately half that of the isogenic normal iPSCs (Figure 1D), suggesting the occurrence of NMD. We further conducted a western blot analysis of OPA1 proteins and found that the two OPA1 protein isoforms obviously diminished in c.2708_2711delTTAG iPSCs compared to isogenic normal iPSCs (Figure 1E), consistent with expression decrease resulting from NMD.

Differentiation of RGCs from iPSCs via 3D retinal organoids

To investigate the possible developmental and functional defects of RGCs caused by the c.2708_2711delTTAG variant, we induced 3D retinal organoids from mutant and isogenic control iPSCs using a previously reported procedure (Kuwahara et al., 2015) (Figure S5A). By days 30–35 of induction culture, layered optic cup retinal organoids were formed from both control and mutant iPSCs, and GFP fluorescence started to emerge within the inner layer of the organoid (Figure S5B), indicating the onset of RGC differentiation. By day 60, GFP fluorescence had spread to the inner layer of the entire retinal organoid (Figure S5B).

In 60-day retinal organoids derived from either control or mutant iPSCs, sectional immunofluorescence staining showed that GFP was colocalized with RGC markers POU4F2, HUC/D, or PAX6 in the inner layer (ganglion cell layer) (Figure 2), confirming GFP^+ cells as RGCs. Quantification of $POU4F2^+$, HUC/D^+, or $PAX6^+$ cells within the inner layer showed that they were reduced by ~30% in the mutant organoid compared to the control (Figure 2), suggesting a possible RGC differentiation defect. $OTX2^+$ and CRX^+ cells were located mostly at the outer edge of the retinal organoids, representing photoreceptor precursors (Figure 2). A small number of cells displayed the expression of recoverin (RCVRN), indicating the generation of cone cells (Figure 2). We detected no significant difference in the number of these marker-positive cells between control and mutant organoids (Figure 2). Most of the cells within the outer layer of retinal organoids should be retinal progenitor cells (RPCs), and indeed, as expected, expressed RPC markers PAX6 and SOX2 as well as the proliferation marker MKI67 (Figure 2). Quantification further showed that $MKI67^+$ cells were decreased by ~14% in the mutant organoid, whereas $SOX2^+$ cells exhibited no significant change (Figure 2). Therefore, at a gross level, both the mutant and control iPSCs are able to form retinal organoids capable of differentiation, but RGC differentiation and RPC proliferation may be affected by the c.2708_2711delTTAG variant.

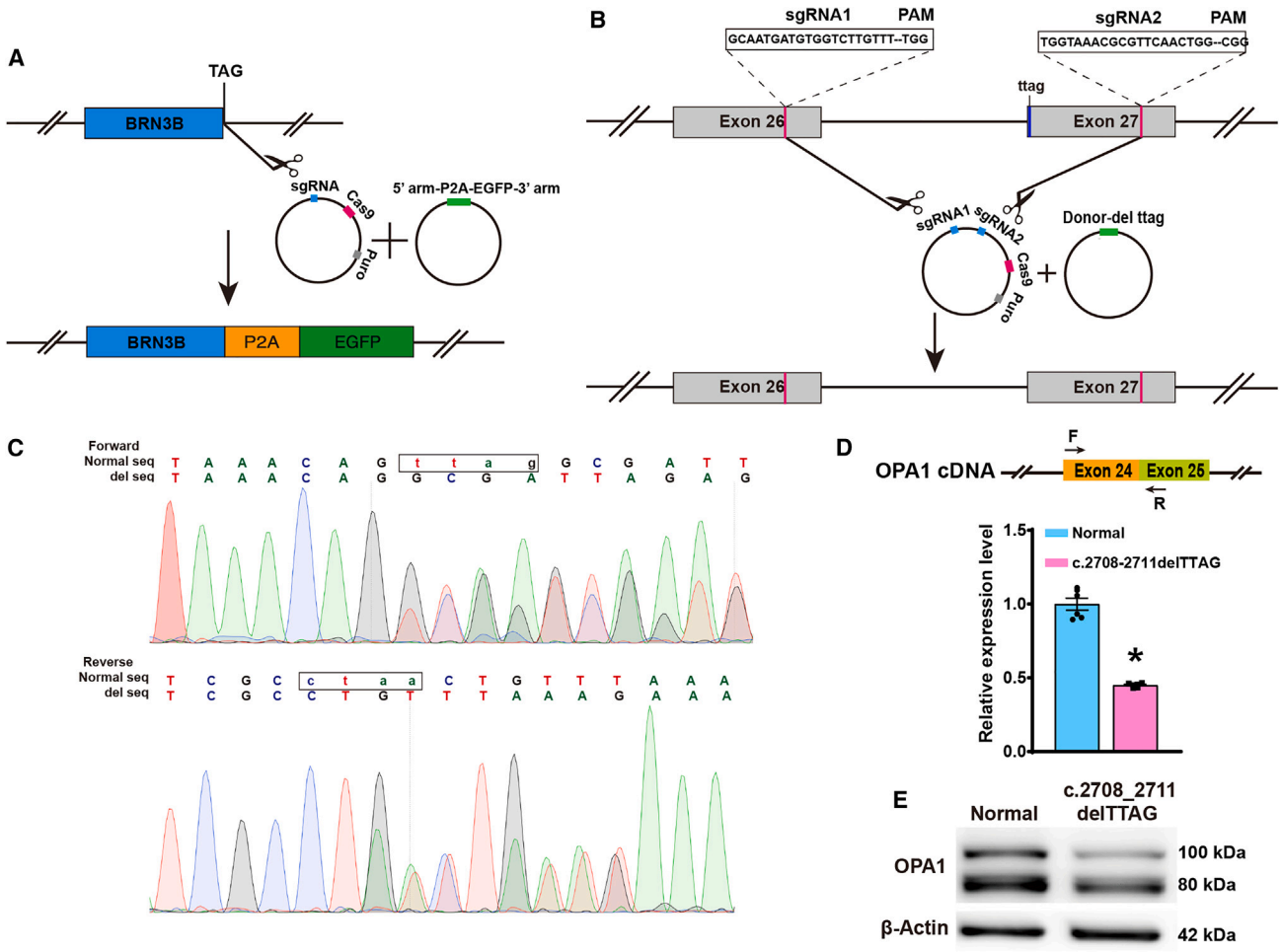

Figure 1. Generation and characterization of BRN3B-GFP-tagged human iPSCs carrying the *OPA1* c.2708_2711delTTAG mutant variant

(A) Schematic illustration depicting the BRN3B-P2A-EGFP reporter design. The CRISPR-Cas9 gene editing technology was used to target the stop codon of *BRN3B* in normal donor iPSCs.

(B) Schematic illustration depicting the gene editing process to generate the c.2708_2711delTTAG variant in normal donor iPSCs carrying the BRN3B-P2A-EGFP reporter.

(C) Peak plots of nucleic acid sequences after successful editing to obtain the c.2708_2711delTTAG variant. Doublet peaks following TTAG after forward and reverse sequencing indicate that the sequenced cell line is heterozygous for the variant.

(D) qRT-PCR analysis confirmed downregulation of *OPA1* mRNA in c.2708_2711delTTAG iPSCs compared with normal iPSCs. The positions of the forward (F) and reverse (R) PCR primers are indicated. Data are presented as mean ± SEM (n = 6, each n represents ~10^6 iPSCs and the experiment was repeated independently 6 times). *$p < 0.0001$.

(E) Representative western blot of OPA1 expressed in normal and c.2708_2711delTTAG iPSCs. β-Actin served as the internal protein control.

Defective RGC differentiation caused by the *OPA1* mutant variant

Unlike 2D culture, the induction of retinal organoids well recapitulates *in vivo* retinal development (Eiraku et al., 2011; Nakano et al., 2012; O'Hara-Wright and Gonzalez-Cordero, 2020; Volkner et al., 2016; Zhang et al., 2021). Thus, the fact that mutant iPSCs were capable of forming retinal organoids provided an opportunity to assess the effect of the c.2708_2711delTTAG variant on RGC differentiation in an environment closely resembling that in the organism. Single-cell transcriptomics has been demonstrated to be an excellent approach to reveal and track cell lineage trajectories during development (Wu et al., 2021). We, therefore, carried out single-cell RNA-sequencing (scRNA-seq) analyses of 60-day retinal organoids to evaluate possible RGC differentiation defects. After removing

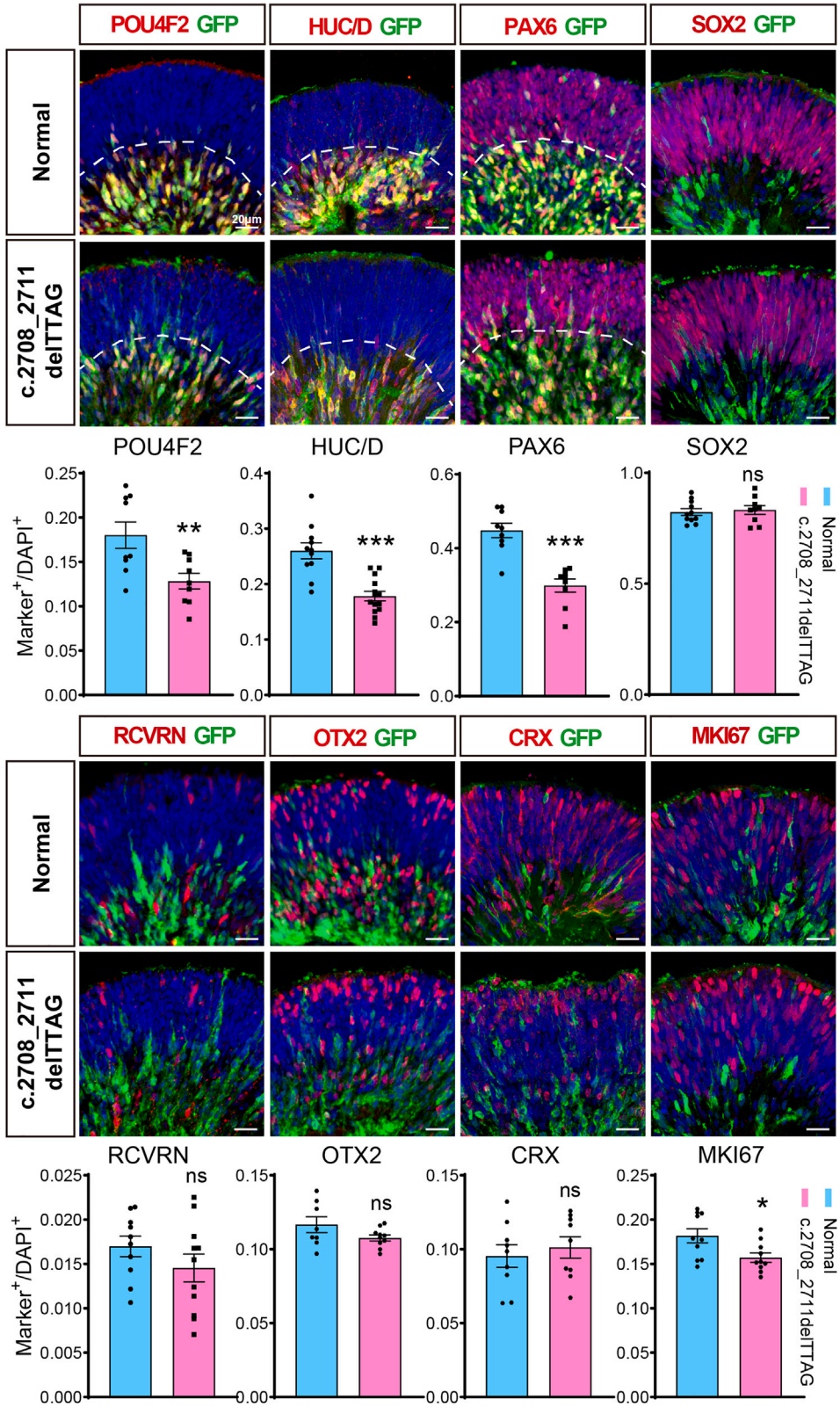

(legend on next page)

doublet cells, we performed a random downsampling to obtain the expression data of 15,145 cells each for the mutant and control organoids to compare the equal number of cells between the 2 groups. Unsupervised combined with marker-based uniform manifold approximation and projection (UMAP) clustering analysis by Seurat 4 (Stuart et al., 2019) yielded 5 clusters of single cells (c1–c5), corresponding to the naive RPCs (nRPCs), transitional RPCs (tRPCs), RGC trajectory, photoreceptor cell (PC) trajectory, and amacrine/horizontal cell (AHC) trajectory, respectively (Figure 3A). Violin plots showed the expression of RPC markers *SOX2* and *VSX2* in clusters c1 and c2, RGC markers *ATOH7*, *POU4F2*, *NEFM*, and *NELL2* in cluster c3; photoreceptor markers *OTX2*, *CRX*, *NRL*, and *PRDM1* in cluster c4; and AHC markers *PTF1A*, *PRDM13*, *TFAP2A*, and *TFAP2B* in cluster c5 (Figure 3C); this validated the identity of these clusters. Pseudotime trajectory analysis further revealed that the RGC, PC, and AHC trajectories were developmentally more advanced than and originated from tRPCs and nRPCs (Figure 3B).

Comparison of mutant and control organoid cells showed that there were similar or even more cells in clusters c3–c5 of the mutant organoid compared to those of the control (Figures 3D and 3E), indicating that mutant RPCs have the potential to differentiate into multiple retinal cell lineages and that the c.2708_2711delTTAG variant may not affect retinal cell fates, including the RGC fate. To further investigate RGC differentiation, we calculated differentially expressed (DE) genes in cluster c3 (RGC trajectory) between the mutant and control organoids and identified 350 genes significantly downregulated in the mutant (Figure 3F; Table S1). Gene Ontology (GO) enrichment analysis showed that these downregulated genes were enriched for GO terms associated with RGC development such as regulation of nervous system development, regulation of neurogenesis, and regulation of cell development, as well as RGC function such as axonogenesis, axon extension, and neuron projection extension (Figure 3G). Close examination of DE genes revealed that a series of known RGC marker genes were downregulated in the mutant (Table S1), suggesting that RGCs fail to differentiate properly in the mutant retinal organoid. Violin and feature plots showed that in cluster c3 of the mutant organoids, there was obvious downregulation in the expression of RGC developmental regulatory genes such as *ATOH7*, *POU4F2*, *ISL1*, *EBF1*, *ONECUT2*, and *PAX6*; typical RGC marker genes, including *SNCG*, *NEFM*, *NELL2*, *ELAVL3*, and *ELAVL4*; and other lesser known RGC marker genes, including *SYT4*, *SYT7*, *SLC38A1*, *C1QL1*, and *RAB31* (Figures 3H and 3I). The downregulation of RGC marker genes in 60-day mutant organoids was further confirmed by qRT-PCR analysis (Figure 3J), consistent with the observed decrease in RGCs immunoreactive for POU4F2, HUC/D, or PAX6 in the mutant organoid (Figure 2).

There were 217 significantly upregulated DE genes in cluster c3 of the mutant organoid (Figure 3F; Table S1). GO enrichment analysis of these genes showed that they were enriched for GO terms including pattern specification process, regionalization, ATP/ADP metabolic process, and ribosome biogenesis (Figure S6A). These upregulated DE genes include some little-expressed RGC-specific genes (e.g., *HOXB5*, *HOXB8*), as well as many more broadly expressed ones (e.g., *TUBB2A*, *DHRS3*) (Figures S6B and S6C). The existence of upregulated genes in mutant RGCs implies their improper differentiation. Thus, together, these results suggest that RGCs are generated but unable to undergo appropriate differentiation in mutant retinal organoids.

Mitochondrial dysfunction in *OPA1* mutant retinal organoids

The mutation of OPA1, a key mitochondrial protein, is expected to cause mitochondrial deficits. We therefore examined mitochondrial phenotypes in mutant retinal organoid cells. DE genes between all mutant and control organoid cells were determined by Seurat from the scRNA-seq dataset (Figure 4A; Table S2), and GO enrichment analysis was performed for all of the DE genes. Interestingly, they were enriched for GO terms such as mitochondrial transport and protein localization to mitochondrion (Figure 4B), suggesting that the c.2708_2711delTTAG variant may affect the expression of mitochondrion-related genes. Close examination of the DE gene list revealed a number of mitochondrial marker genes significantly downregulated in mutant organoid cells (Table S2). Violin and feature plots showed that in nearly all of the cell clusters, including RGCs, in

Figure 2. Expression and quantification of progenitor, precursor, and cell-type markers in retinal organoids

Sections from 60-day retinal organoids derived from normal and c.2708_2711delTTAG iPSCs were double-immunostained with an anti-GFP antibody and those against the indicated protein markers, and counterstained with DAPI. In both normal and mutant organoids, there were RGCs (POU4F2$^+$, HUC/D$^+$, or PAX6$^+$), amacrine cells (HUC/D$^+$ or PAX6$^+$), cone cells (RCVRN$^+$), photoreceptor precursor cells (OTX2$^+$ or CRX$^+$), RPCs (SOX2$^+$ or PAX6$^+$), and proliferative RPCs (MKI67$^+$). The quantification data of RGCs, identified by the markers POU4F2, HUC/D, or PAX6, were expressed as the proportion of positive cells in all DAPI-labeled nuclei within the inner layer (outlined by dashed lines) of the organoid. Other cell types were quantified from all of the layers of the organoid. All of the data are presented as mean ± SEM (n = 8–14 individual organoids from at least 2 independent organoid batches). ns, not significant; *p < 0.05; **p < 0.01; ***p < 0.0001. Scale bar: 20 μm.

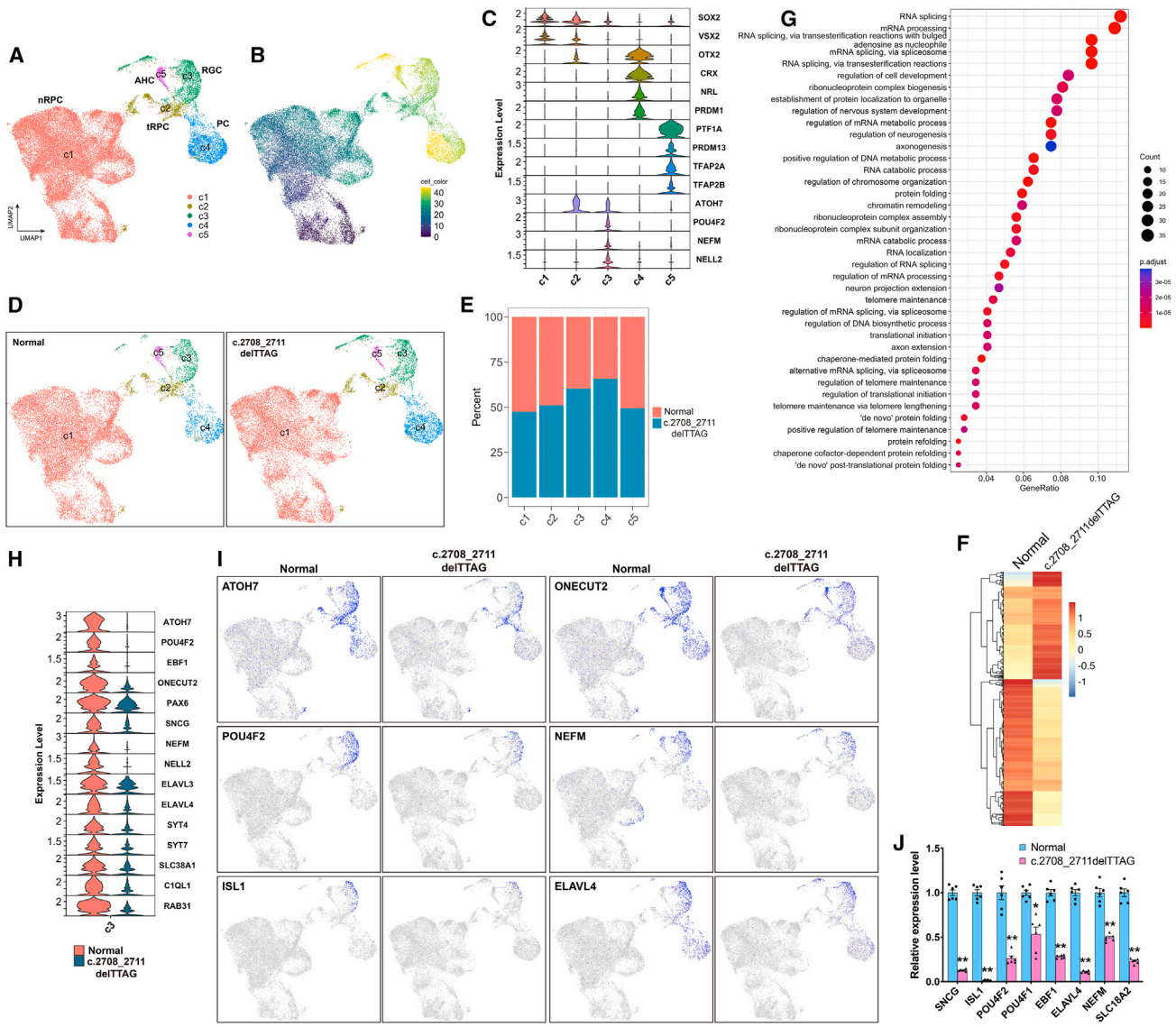

Figure 3. Single-cell transcriptome profiling reveals RGC differentiation defects in 60-day retinal organoids derived from c.2708_2711delTTAG iPSCs

(A) UMAP plot of single cells from normal and mutant retinal organoids resulting from unsupervised combined with marker-based clustering analysis.

(B) Pseudotime trajectories of the sequenced retinal organoid cells.

(C) Stacked violin plot showing expression patterns of the indicated retinal cell marker genes in single-cell clusters (c1–c5).

(D) Comparison of UMAP plots of equal number of single cells from normal and mutant retinal organoids.

(E) Proportion of cell numbers in each cell cluster of normal and mutant retinal organoids.

(F) Expression heatmap of differentially expressed genes in cluster c3 between normal and mutant retinal organoids.

(G) GO term enrichment analysis of significantly downregulated genes in the c3 cluster (RGC trajectory) of the mutant retinal organoid.

(H and I) Stacked violin plot and feature plots showing expression patterns of the indicated RGC developmental regulatory genes and RGC marker genes in the c3 cluster of normal and mutant retinal organoids.

(J) qRT-PCR analysis confirming downregulation of the indicated RGC marker genes in 60-day mutant retinal organoids. Data are presented as mean ± SEM (n = 6, each n represents ~60 retinal organoids from 3 independent organoid batches and the experiment was repeated independently 6 times). *p < 0.0005; **p < 0.0001.

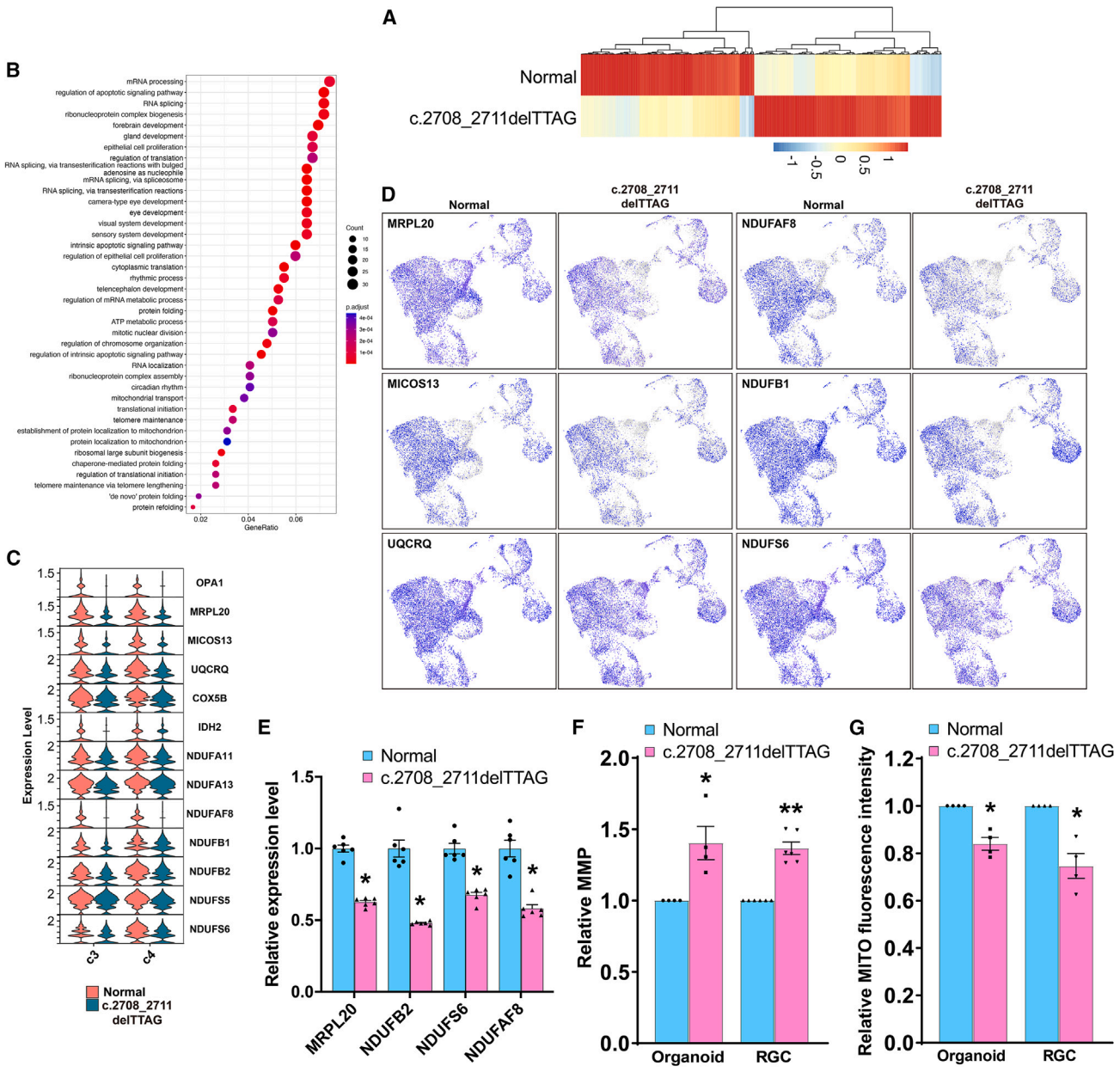

Figure 4. Mitochondrial dysfunction in 60-day retinal organoids derived from c.2708_2711delTTAG iPSCs

(A) Expression heatmap of differentially expressed genes between normal and mutant retinal organoid cells.

(B) GO term enrichment analysis of differentially expressed genes between normal and mutant retinal organoids.

(C and D) Stacked violin plot and feature plots showing expression patterns of the indicated mitochondrial marker genes in normal and mutant retinal organoid cells.

(E) qRT-PCR analysis confirming downregulation of the indicated mitochondrial marker genes in mutant retinal organoids. Data are presented as mean ± SEM (n = 6, each n represents ~60 retinal organoids from 3 independent organoid batches and the experiment was repeated independently 6 times). *p < 0.0001.

(F and G) Relative MMP and Mito-Tracker Red fluorescence intensity in normal and mutant retinal organoid cells and enriched RGCs. Data are presented as mean ± SEM (n = 4–6, each n represents ~60 retinal organoids from 3 independent organoid batches and the experiment was repeated independently 4–6 times). *p < 0.05; **p < 0.0001.

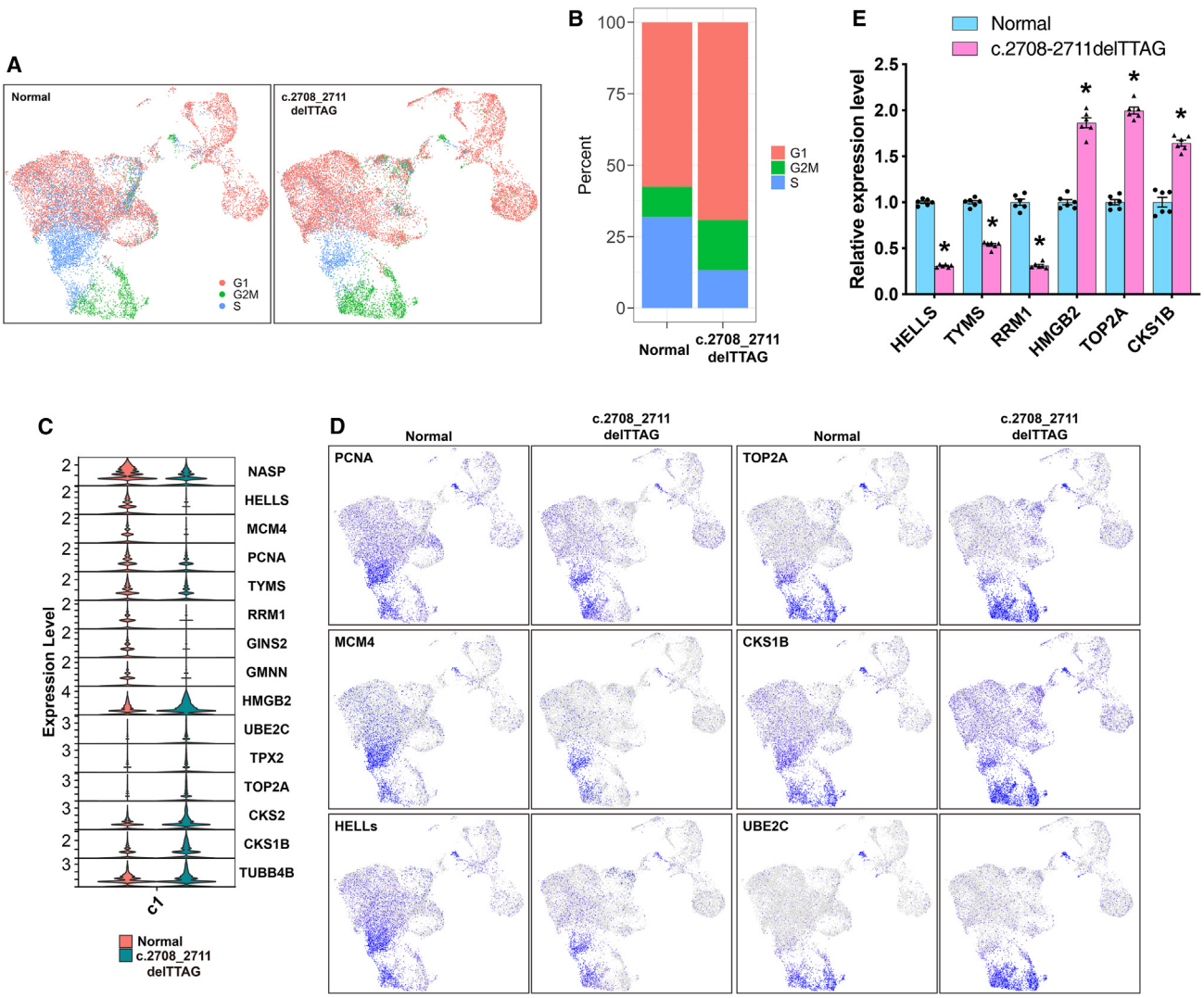

Figure 5. Diminished retinal progenitor proliferation in 60-day retinal organoids derived from c.2708_2711delTTAG iPSCs

(A and B) Cell-cycle analysis showing a decrease in the proportion of cells distributed in S phase but an increase in that distributed in G2/M phase in the mutant retinal organoid.

(C and D) Stacked violin plot and feature plots showing expression patterns of the indicated S phase marker genes (*NASP*, *HELLS*, *MCM4*, *PCNA*, *TYMS*, *RRM1*, *GINS2*, and *GMNN*) and G2/M phase marker genes (*HMGB2*, *UBE2C*, *TPX2*, *TOP2A*, *CKS2*, *CKS1B*, and *TUBB4B*) in the c1 cluster of normal and mutant retinal organoids.

(E) qRT-PCR analysis confirming expression alterations of the indicated cell-cycle marker genes in mutant retinal organoids. Data are presented as mean ± SEM (n = 6, each n represents ~60 retinal organoids from 3 independent organoid batches and the experiment was repeated independently 6 times). *p < 0.0001.

c3 of the mutant organoid, there was downregulation in the expression of many mitochondrial marker genes, including *MRPL20*, *MICOS13*, *UQCRQ*, *NDUFAF8*, *NDUFB1*, and *NDUFS6* (Figures 4C and 4D). The downregulation of *MRPL20*, *NDUFB2*, *NDUFS6*, and *NDUFAF8* was further validated by qRT-PCR assay (Figure 4E), indicating that OPA1 may be able to directly and/or indirectly regulate the expression of many mitochondrial genes.

The mitochondrial membrane potential (MMP) is an indicator of mitochondrial function and physiology; therefore, we measured MMP in 60-day control and mutant retinal organoid cells. Compared to control cells, there was ~40.4% and 36.8% increases in MMP in total mutant organoid cells and enriched mutant RGCs, respectively (Figure 4F). These increases in MMP were further validated in single cultured mutant RGCs (Figure S7), suggesting that

the *OPA1* c.2708_2711delTTAG mutant variant may indeed cause mitochondrial dysfunction. Consistent with this, total mutant organoid cells and enriched mutant RGCs also exhibited diminished MitoTracker Red fluorescence compared to control cells (Figure 4G).

Reduced retinal progenitor proliferation in *OPA1* mutant retinal organoids

Apart from mitochondrion-related GO terms, DE genes between mutant and control organoid cells were also enriched for GO terms such as mitotic nuclear division, epithelial cell proliferation, and regulation of epithelial cell proliferation (Figure 4B), suggesting that the *OPA1* c.2708_2711delTTAG mutant variant may affect RPC proliferation. In addition, we observed diminished MKI67 immunoreactivity in mutant organoids (Figure 2), and there was a small decrease in nRPCs in cluster c1 of the mutant organoid compared to the control (Figures 3D and 3E). Therefore, we performed a cell-cycle analysis of the sequenced single cells by Seurat using 70 cell-cycle markers (Nestorowa et al., 2016). This analysis showed that compared to the control, in the mutant organoid, RPCs at the S phase dropped from 31.9% to 13.2%, whereas G2/M RPCs increased from 10.6% to 17.6% and G1/G0 cells increased from 57.6% to 69.2% (Figures 5A and 5B). Consistent with this, there were a number of cell-cycle marker genes in the DE gene list (Table S2). Violin and feature plots showed that in cluster c1 (nRPCs) of the mutant organoids, there was obvious downregulation of S marker genes such as *HELLS*, *MCM4*, *PCNA*, and *GINS2* but upregulation of G2/M marker genes such as *HMGB2*, *UBE2C*, *TOP2A*, and *CKS1B* (Figures 5C and 5D). Using a qRT-PCR assay, we validated the downregulation of *HELLS*, *TYMS*, and *RRM1* and the upregulation of *HMGB2*, *TOP2A*, and *CKS1B* in mutant organoid cells (Figure 5E). Despite decreased S cells, as aforementioned, we observed elevated G1/G0 and G2/M cells as well as an increase in cells in clusters c3 and c4 (RGC and PC lineages) in the mutant organoid (Figures 3D and 3E), suggesting that the c.2708_2711delTTAG variant may also accelerate cell-cycle exit.

Morphological and physiological deficits in *OPA1* mutant RGCs

It has been shown that RGC injury and disease result in RGC morphological abnormalities such as dendritic remodeling and diminished soma size (Agostinone et al., 2018; Kalesnykas et al., 2012; VanderWall et al., 2020). To investigate whether the *OPA1* c.2708_2711delTTAG mutant variant causes a similar phenotype, we purified RGCs from 60-day control and mutant retinal organoids by fluorescence-activated cell sorting (FACS), and then cultured them in neuronal differentiation medium for 2 weeks to let them undergo terminal differentiation and maturation. RGCs were visualized by GFP immunofluorescence, and their morphometric measurements were carried out (Figure 6A). This analysis revealed that compared to control RGCs, mutant RGCs had smaller somas and shorter neurites (Figures 6B and 6C), and they were less complex (Figure 6D), indicative of morphological and differentiation defects. Given the observed downregulation of RGC transcription factors (e.g., POU4F2, EBF1), cytoskeletal components (e.g., NEFL, NEFM), neuronal RNA splicing factors (e.g., ELAVL3, ELAVL4), and synaptic components (e.g., SYT4, SYT7) in the mutant retinal organoids (Figures 3H and 3I), it appears that the c.2708_2711delTTAG variant may impair both initial and terminal RGC differentiation.

To investigate whether the observed differentiation defects led to changes in functional maturity and physiological properties, we performed whole-cell patch clamp recordings of control and mutant RGCs (Figure 7A). In this experiment, normal and c.2708_2711delTTAG RGCs FACS-purified from 60-day retinal organoids were cultured in neuronal differentiation medium for 2 weeks. We found that all of the recorded control and mutant RGCs displayed single or multiple firings in response to current injection (Figures 7A–7C; normal RGCs: n = 36, single/multiple = 10/26; mutant RGCs: n = 37, single/multiple = 16/21). Another important aspect of neuronal network maturity is spontaneous action potential (sAP) firing that is defined as those reaching a membrane potential above 0 mV. Among all of the recorded RGCs, 47.2% and 56.8% of control and mutant RGCs, respectively, generated typical spontaneous APs when the resting membrane potential was maintained at ∼−60 mV (Figures 7A and 7D). Moreover, spontaneous postsynaptic current (sPSC) responses, as evidence of synaptic connectivity, were obtained in a portion of the recorded RGCs (Figure 7F; normal: 11/36 versus mutant: 13/37). Although the average capacitance of control RGCs and mutant ones was not significantly different (22.28 ± 9.0 pF, n = 27 versus 22.27 ± 7.4 pF, n = 31), the mutant RGCs exhibited a significant decrease in the peak amplitude of voltage-activated sodium currents and outward potassium currents under voltage-step injection (Figures 7G and 7H); and no significant changes were observed in the AP thresholds in current-clamp recording (Figure 7I). Therefore, the c.2708_2711delTTAG mutant variant affects not only the differentiation program of RGCs but also their electrophysiological properties.

DISCUSSION

In this study, the pathogenic mechanism of a haploinsufficient *OPA1* mutation was investigated in RGCs using retinal organoids for the first time. Isogenic iPSCs carrying the hotspot *OPA1* c.2708_2711delTTAG mutation were

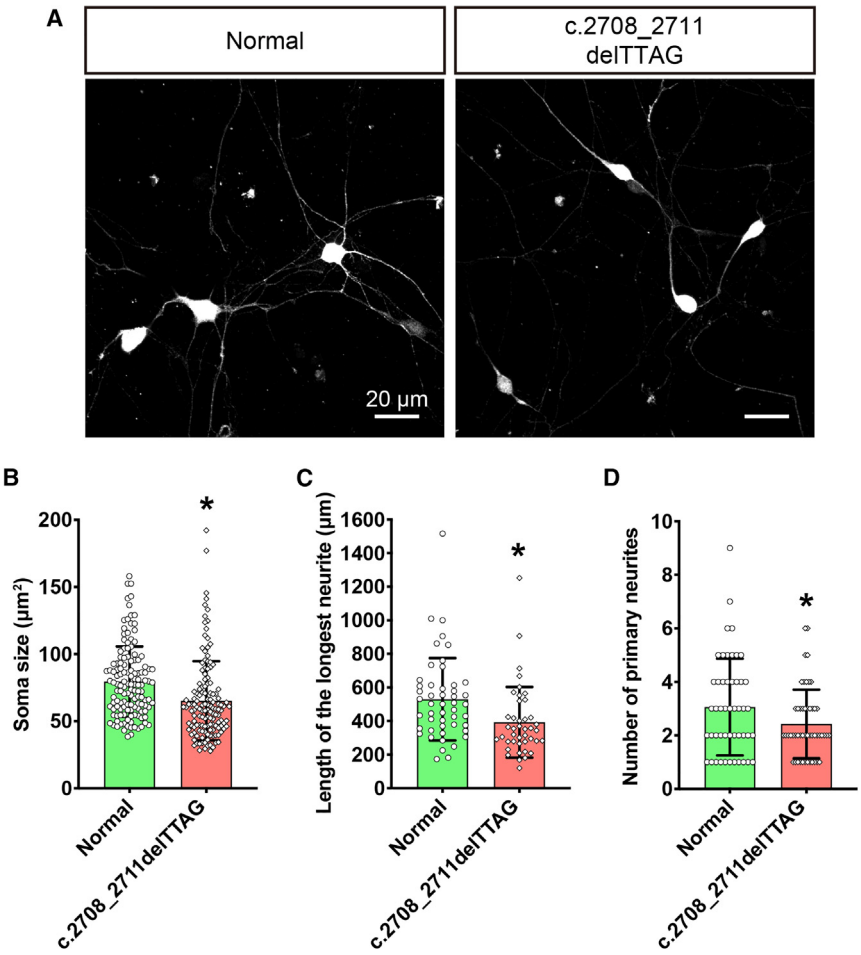

Figure 6. Morphological changes in RGCs derived from c.2708_2711delTTAG iPSCs

(A) RGCs purified from 60-day normal and mutant retinal organoids were cultured in neuronal differentiation medium for 2 weeks and then were labeled by immunofluorescence with an anti-GFP antibody. Scale bars: 20 μm.

(B) The soma area of the mutant RGCs is significantly decreased. Data are presented as mean ± SD (normal, 134 cells, and c.2708_2711delTTAG, 138 cells; both from 3 independent organoid batches). *$p < 0.0001$.

(C) The length of the longest neurite of the mutant RGCs is significantly shortened. Data are presented as mean ± SD (normal, 49 cells, and c.2708_2711delTTAG, 42 cells; both from 3 independent organoid batches). *$p < 0.01$.

(D) There is a significant reduction in the number of primary neurites in mutant RGCs, which indicates decreased complexity. Data are presented as mean ± SD (normal, 49 cells, and c.2708_2711delTTAG, 52 cells; both from 3 independent organoid batches). *$p < 0.05$.

generated by CRISPR-Cas9 gene editing from normal iPSCs harboring the BRN3B-GFP RGC reporter. The 3D retinal organoids were subsequently induced from these mutant iPSCs, wherein RGCs were shown to be generated but unable to undergo appropriate differentiation by a combination of molecular, cellular, and scRNA-seq analyses. Further morphometric measurements and whole-cell patch clamp recording revealed that mature mutant RGCs had smaller somas, shorter neurites, less complexity, and smaller peak amplitudes of voltage-activated sodium currents and outward potassium currents compared to control RGCs, suggesting that the *OPA1* mutation impairs both the initial and terminal RGC differentiation. In addition, mutant organoids displayed increased MMP, diminished mitochondrial content, and downregulation of a variety of mitochondrial marker genes, suggesting that the *OPA1* mutant variant causes mitochondrial dysfunction. It is interesting that scRNA-seq and cell-cycle analyses revealed an unexpected effect of the c.2708_2711delTTAG mutation on RPCs; it may not only repress the proliferation of RPCs but also accelerate their cell-cycle exit.

One major goal of this work was to model ADOA with 3D retinal organoids to settle the issue of whether haploinsufficient *OPA1* mutations perturb RGC development, and we have demonstrated that they in fact cause RGC differentiation defects. Previously, opposing conclusions were reached about the effect of haploinsufficient *OPA1* mutations on RGC differentiation based on 2D differentiation procedures (Chen et al., 2016). Although it was unclear what exactly caused this discrepancy, we reasoned that compared to 2D culture, 3D retinal organoids would provide a much more reliable model to resolve the issue. Therefore, we generated by CRISPR-Cas9 gene editing an isogenic iPSC line carrying the hotspot haploinsufficient *OPA1* mutant variant c.2708_2711delTTAG from a normal human iPSC line harboring BRN3B-GFP, which was knocked in also by gene editing. The generation of isogenic lines provides a valuable means of analyzing disease phenotypes associated with relevant mutations, because it reduces genetic variability between cell lines and establishes a more consistent platform for analysis. Moreover, we made use of another advanced technology, single-cell

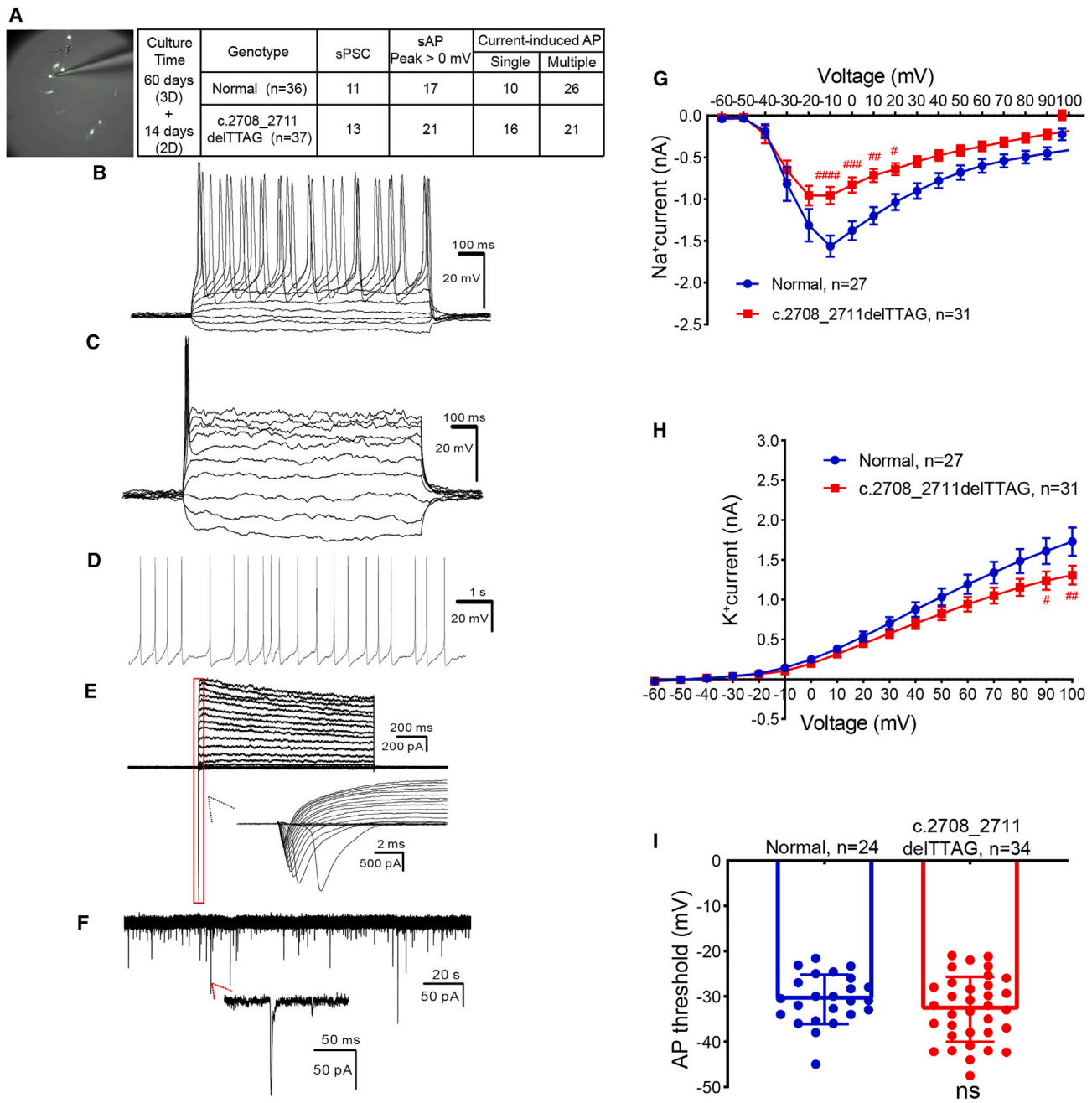

Figure 7. Electrophysiological properties of RGCs derived from c.2708_2711delTTAG iPSCs

(A) A merged micrograph showing patch-clamp recording of a typical GFP$^+$ RGC and a summary of the electrophysiological properties of the recorded control and mutant cells. Before recording, normal and mutant RGCs were purified by FACS from retinal organoids after 60 days of suspension culture (3D) and then cultured (2D) in neuronal differentiation medium for 2 weeks.

(B and C) All of the recorded RGCs from both groups exhibited single (C) or multiple (B) APs under current injection (normal, n = 36 cells; mutant, n = 37 cells; both from at least 3 independent organoid batches).

(D) Representative current-clamp recording from a spontaneously active RGC (V_m = −60 mV) (normal, n = 17 cells; mutant, n = 21 cells). V_m, voltage of cell membrane.

(E) RGCs from both groups exhibited voltage-activated sodium and potassium currents in response to voltage step stimuli (normal, n = 27 cells; mutant, n = 31 cells).

(legend continued on next page)

transcriptomics, which has been shown to be an excellent tool for visualizing and tracking cell lineage trajectories during retinal development (Wu et al., 2021). These approaches in combination have allowed us to conclude with confidence that although both the control and mutant iPSCs were able to form retinal organoids capable of differentiation into RGCs and photoreceptors, the mutant *OPA1* variant caused deficiency in the initial and terminal differentiation processes of RGCs, indicating little effect of the hotspot *OPA1* mutant on the fates of RGCs and other cell types. However, the produced RGCs appeared unable to undergo proper differentiation because the expression of a variety of RGC marker genes was downregulated in these cells. Moreover, prolonged differentiation of RGCs isolated from the organoids revealed that mutant RGCs had smaller somas and shorter neurites and were less complex, suggesting that they are defective in terminal differentiation as well. Thus, our data together demonstrate that the haploinsufficient *OPA1* c.2708_2711delTTAG mutant variant does not cause a complete failure in RGC differentiation, nor does it have no effect on RGC differentiation, as reported previously (Chen et al., 2016; Sladen et al., 2022), which more closely manifest the ADOA symptoms. This outcome reinforces the notion that retinal organoids are more suitable than 2D differentiation for modeling ADOA *in vitro*.

Mitochondria are dynamic organelles that maintain their morphology in steady states via fission and fusion of mitochondrial membranes (Tilokani et al., 2018). Mitochondrial dynamics has been demonstrated to regulate the stem cell fate, maintenance of the pluripotent state of stem cells, and differentiation of stem cells into other cell types (Chakrabarty and Chandel, 2021; Khacho et al., 2019; Noguchi and Kasahara, 2018; Zhang et al., 2018). For instance, naive mouse embryonic stem cells (mESCs) display fragmented and globular mitochondria, whereas primed epiblast stem cells display elongated mitochondria (Zhou et al., 2012). It was reported that inducing mitochondrial fusion could drive the exit of ESCs from the naive state (Bahat et al., 2018). Mitochondrial fusion is also crucial for the differentiation of stem cells. Lowering the levels of mitochondrial membrane fusion-mediating proteins MFN2 and OPA1 by gene trapping was found to impair the differentiation of mESCs into functional beating cardiomyocytes (Kasahara et al., 2013). Similarly, MFN2 knockdown inhibits the differentiation and synaptogenesis of human iPSC-derived cortical neurons (Fang et al., 2016), and reduced OPA1 expression perturbs GABAergic neuronal development by neural progenitor cells (Caglayan et al., 2020). Mitochondria appear to control the differentiation process by multiple mechanisms, including acting as a hub to coordinate signaling pathways such as NOTCH and WNT signaling and by relying on their metabolites to regulate chromatin/protein modifications (Noguchi and Kasahara, 2018; Zhang et al., 2018). Our observation that the *OPA1* c.2708_2711delTTAG mutant variant causes RGC differentiation defects is in line with previous findings that mitochondrial dysfunction impairs the differentiation of other cell types. It will be interesting to delineate the detailed underlying mechanism in the future.

Apart from the impact on RGC differentiation, retinal organoids have helped to uncover an unexpected effect of *OPA1* haploinsufficiency on RPC proliferation, which may indirectly influence retinal cell development. Cell-cycle analysis of sequenced single cells revealed a reduction of RPCs in S phase but an increase of RPCs in G2/M and G1/G0 phases in the mutant organoid, which were validated by the downregulation of S marker genes and upregulation of G2/M marker genes, implying that the *OPA1* mutant variant may not only inhibit the proliferation of RPCs but also accelerate their cell-cycle exit. Therefore, the unaltered or more number of cells present in the RGC, photoreceptor, and AHC trajectories of the mutant organoid may be the net result of these two opposing effects on the cell cycle. Presumably, the effect of *OPA1* mutation on RPC cell cycle could result from dynamic and metabolic changes in mitochondria or through regulating cell-cycle control genes via DNA methylation (Caglayan et al., 2020). Compared to previous studies, another new insight we have gained from the present study is that even after being subject to prolonged terminal differentiation culture, mutant RGCs are physiologically abnormal, most likely due to their inability to properly differentiate. Therefore, whole-cell patch clamp recording showed that mutant RGCs had smaller peak amplitudes of voltage-activated sodium currents and outward potassium currents. Electrophysiological deficit may be a common pathology of degenerating RGCs. A previous study showed that organoid-derived RGCs carrying the OPTN(E50K) glaucomatous mutation had elevated excitability (VanderWall et al., 2020).

The intricate nature of mitochondrial diseases stems from their dual genetic origin, whereby the proteins of the organelle are encoded by both nuclear and mitochondrial genomes. The inherent instability of mtDNA is known to be a key contributor to the pathophysiology

(F) Representative traces showing sPSCs of cultured RGCs derived from iPSCs (normal, n = 11 cells; mutant, n = 13 cells).
(G and H) Compared with normal RGCs, mutant RGCs displayed significantly decreased peak amplitude of voltage-activated sodium currents and potassium currents. Data are presented as mean ± SEM. #p < 0.05; ##p < 0.005; ###p < 0.0005; ####p < 0.0001.
(I) The c.2708_2711delTTAG mutation had no significant effect on AP thresholds. Data are presented as mean ± SD.

of age-related disorders, degenerative diseases, and cancer (Chinnery et al., 2002). Therefore, prior investigations of *OPA1*-caused pathogenesis have primarily centered on the mitochondrial function and mtDNA content (Sladen et al., 2022; Zanna et al., 2008), with little emphasis on whether the haploinsufficient *OPA1* mutations also affect nuclear genes that are required for mitochondrial function. In this work, our investigation revealed a downregulation in the expression of the nuclear gene *MRPL20* in the *OPA1* mutant organoid, which encodes a mitochondrial ribosomal protein large subunit that facilitates protein synthesis within the mitochondrion (Cheong et al., 2020). In addition, the reduced expression of *NDUFB2*, *NDUFS6*, and *NDUFAF8* in the mutant organoid suggests that the c.2708_2711delTTAG mutation disrupts the synthesis and assembly of subunits of ubiquinone oxidoreductase (i.e., mitochondrial complex I) (Stroud et al., 2016), which would subsequently impair its function and activity. The downregulation of these nuclear genes would impede mitochondrial function, which, when coupled with the decline in mitochondrial content observed in mutant organoids, would presumably culminate in the loss of energy supply to and eventual deterioration of RGCs.

The present study has leveraged the 3D retinal organoid as a superior model system to investigate the effect of a haploinsufficient *OPA1* mutation on RGC pathogenesis. In particular, our work provides an excellent example to show that the organoid technology combined with CRISPR-Cas9 gene editing serves as a powerful approach to definitively identify developmental and functional phenotypes associated with gene mutations. Gene editing in this case allowed for the specific deletion of TTAG of the *OPA1* c.2708_2711delTTAG mutant variant in the isogenic iPSC line, thereby eliminating interindividual genetic variability and ensuring reliable and definitive characterization of disease-related phenotypes. Similar approaches have been used to successfully model and/or correct gene mutations that cause retinitis pigmentosa or glaucoma (Deng et al., 2018; VanderWall et al., 2020). Aside from disease modeling, 3D organoids are quite amenable to drug testing and screening, as demonstrated for those induced from primary hepatocytes (Broutier et al., 2017). Previously, under 2D differentiation conditions, iPSCs carrying a haploinsufficient *OPA1* mutation were shown to be incapable of differentiating into RGCs; however, treatment with Noggin or 17β-estradiol was able to rescue the phenotype (Chen et al., 2016). Although it remains to be determined whether these two molecules are also effective for rescuing RGC differentiation defects in 3D retinal organoids, these provide promising precedents for discovering potential ADOA therapeutics through drug screening using retinal organoids.

EXPERIMENTAL PROCEDURES

For further details, see the supplemental experimental procedures.

Resource availability

Corresponding author

Mengqing Xiang: xiangmq3@mail.sysu.edu.cn.

Materials availability

Materials generated in this study are available from the Xiang lab upon request.

Data and code availability

The scRNA-seq data have been deposited in the NCBI Sequence Read Archive database with the accession number PRJNA1000913.

Maintenance of iPSCs

The human iPSCs were maintained according to our previously published protocol (Cheng et al., 2017). The cell lines used in this study were the UiPSC-001 normal human iPSCs (Cheng et al., 2017) and normal iPSCs harboring BRN3B-GFP and mutant iPSCs carrying *OPA1* c.2708-2711delTTAG and BRN3B-GFP obtained by CRISPR/Cas9 gene editing.

Differentiation of retinal organoids from iPSCs

iPSCs were differentiated into retinal organoids as described previously (Kuwahara et al., 2015).

RGC enrichment and differentiation

Single cells were harvested from 60-day normal and *OPA1* c.2807_2811delTTAG mutant retinal organoids. They were resuspended with 1–2 mL Dulbecco's PBS containing 2% fetal bovine serum and 1 mM EDTA. GFP^+ RGCs were then enriched by FACS using the FACSAria Fusion cell sorter (BD Biosciences). Approximately 30,000 cells were plated on a poly-ornithine/laminin-coated coverslip in a well of 24-well plate, cultured in BrainPhys medium (Stem Cell Technology) for 2 weeks, and then fixed in 4% paraformaldehyde for immunocytochemistry. Images were captured with a laser scanning confocal microscope (Carl Zeiss, LSM700) and analyzed using ImageJ software.

scRNA-seq analysis

scRNA-seq analysis was performed as previously described (Liu et al., 2023; Xiao et al., 2020).

SUPPLEMENTAL INFORMATION

Supplemental information can be found online at https://doi.org/10.1016/j.stemcr.2023.11.004.

ACKNOWLEDGMENTS

We thank the staff of the Core Facilities of the State Key Laboratory of Ophthalmology, Zhongshan Ophthalmic Center for technical support. This work was supported in part by the National Natural Science Foundation of China (81970794 and 81721003), the Science and Technology Planning Projects of Guangzhou City (201904020036), "Technology Innovation 2030-Major Projects" on Brain Science and Brain-Like Computing of the Ministry of

Science and Technology of the People's Republic of China (2021ZD0202603), the Local Innovative and Research Teams Project of Guangdong Pearl River Talents Program, the Science and Technology Planning Project of Guangdong Province (2023B1212060018), and the Fundamental Research Funds of the State Key Laboratory of Ophthalmology, Sun Yat-sen University.

AUTHOR CONTRIBUTIONS

M.X. conceived and designed the research. Q.L., K.X., L.C., and M.X. performed the experiments and analyzed the data. M.X., Q.L., and K.X. interpreted the data and wrote the manuscript. All of the authors contributed to the critical reading of the manuscript.

DECLARATION OF INTERESTS

The authors declare no competing interests.

Received: April 22, 2023
Revised: November 15, 2023
Accepted: November 16, 2023
Published: December 14, 2023

REFERENCES

Agostinone, J., Alarcon-Martinez, L., Gamlin, C., Yu, W.Q., Wong, R.O.L., and Di Polo, A. (2018). Insulin signalling promotes dendrite and synapse regeneration and restores circuit function after axonal injury. Brain *141*, 1963–1980.

Alavi, M.V., and Fuhrmann, N. (2013). Dominant optic atrophy, OPA1, and mitochondrial quality control: understanding mitochondrial network dynamics. Mol. Neurodegener. *8*, 32.

Bahat, A., Goldman, A., Zaltsman, Y., Khan, D.H., Halperin, C., Amzallag, E., Krupalnik, V., Mullokandov, M., Silberman, A., Erez, A., et al. (2018). MTCH2-mediated mitochondrial fusion drives exit from naive pluripotency in embryonic stem cells. Nat. Commun. *9*, 5132.

Brogna, S., and Wen, J. (2009). Nonsense-mediated mRNA decay (NMD) mechanisms. Nat. Struct. Mol. Biol. *16*, 107–113.

Broutier, L., Mastrogiovanni, G., Verstegen, M.M., Francies, H.E., Gavarró, L.M., Bradshaw, C.R., Allen, G.E., Arnes-Benito, R., Sidorova, O., Gaspersz, M.P., et al. (2017). Human primary liver cancer–derived organoid cultures for disease modeling and drug screening. Nat. Med. *23*, 1424–1435.

Caglayan, S., Hashim, A., Cieslar-Pobuda, A., Jensen, V., Behringer, S., Talug, B., Chu, D.T., Pecquet, C., Rogne, M., Brech, A., et al. (2020). Optic atrophy 1 controls human neuronal development by preventing aberrant nuclear DNA methylation. iScience *23*, 101154.

Chakrabarty, R.P., and Chandel, N.S. (2021). Mitochondria as signaling organelles control mammalian stem cell fate. Cell Stem Cell *28*, 394–408.

Chen, J., Riazifar, H., Guan, M.-X., and Huang, T. (2016). Modeling autosomal dominant optic atrophy using induced pluripotent stem cells and identifying potential therapeutic targets. Stem Cell Res. Ther. *7*, 2.

Cheng, L., Lei, Q., Yin, C., Wang, H.Y., Jin, K., and Xiang, M. (2017). Generation of urine cell-derived non-integrative human iPSCs and iNSCs: a step-by-step optimized protocol. Front. Mol. Neurosci. *10*, 348.

Cheong, A., Lingutla, R., and Mager, J. (2020). Expression analysis of mammalian mitochondrial ribosomal protein genes. Gene Expr. Patterns *38*, 119147.

Chinnery, P.F., Samuels, D.C., Elson, J., and Turnbull, D.M. (2002). Accumulation of mitochondrial DNA mutations in ageing, cancer, and mitochondrial disease: is there a common mechanism? Lancet *360*, 1323–1325.

Cipolat, S., Martins de Brito, O., Dal Zilio, B., Scorrano, L., and Korsmeyer, S.J. (2004). OPA1 requires Mitofusin 1 to promote mitochondrial fusion. Proc. Natl. Acad. Sci. USA *101*, 15927–15932.

Del Dotto, V., Mishra, P., Vidoni, S., Fogazza, M., Maresca, A., Caporali, L., McCaffery, J.M., Cappelletti, M., Baruffini, E., Lenaers, G., et al. (2017). OPA1 isoforms in the hierarchical organization of mitochondrial functions. Cell Rep. *19*, 2557–2571.

Delettre, C., Griffoin, J.-M., Kaplan, J., Dollfus, H., Lorenz, B., Faivre, L., Lenaers, G., Belenguer, P., and Hamel, C.P. (2001). Mutation spectrum and splicing variants in the OPA1 gene. Hum. Genet. *109*, 584–591.

Deng, W.L., Gao, M.L., Lei, X.L., Lv, J.N., Zhao, H., He, K.W., Xia, X.X., Li, L.Y., Chen, Y.C., Li, Y.P., et al. (2018). Gene correction reverses ciliopathy and photoreceptor loss in iPSC-derived retinal organoids from retinitis pigmentosa patients. Stem Cell Rep. *10*, 2005.

Eiraku, M., Takata, N., Ishibashi, H., Kawada, M., Sakakura, E., Okuda, S., Sekiguchi, K., Adachi, T., and Sasai, Y. (2011). Self-organizing optic-cup morphogenesis in three-dimensional culture. Nature *472*, 51–56.

Fang, D., Yan, S., Yu, Q., Chen, D., and Yan, S.S. (2016). Mfn2 is required for mitochondrial development and synapse formation in human induced pluripotent stem cells/hiPSC derived cortical neurons. Sci. Rep. *6*, 31462.

Gan, L., Xiang, M., Zhou, L., Wagner, D.S., Klein, W.H., and Nathans, J. (1996). POU domain factor Brn-3b is required for the development of a large set of retinal ganglion cells. Proc. Natl. Acad. Sci. USA *93*, 3920–3925.

Ham, M., Han, J., Osann, K., Smith, M., and Kimonis, V. (2019). Meta-analysis of genotype-phenotype analysis of OPA1 mutations in autosomal dominant optic atrophy. Mitochondrion *46*, 262–269.

Heiduschka, P., Schnichels, S., Fuhrmann, N., Hofmeister, S., Schraermeyer, U., Wissinger, B., and Alavi, M.V. (2010). Electrophysiological and histologic assessment of retinal ganglion cell fate in a mouse model for OPA1-associated autosomal dominant optic atrophy. Invest. Ophthalmol. Vis. Sci. *51*, 1424–1431.

Kalesnykas, G., Oglesby, E.N., Zack, D.J., Cone, F.E., Steinhart, M.R., Tian, J., Pease, M.E., and Quigley, H.A. (2012). Retinal ganglion cell morphology after optic nerve crush and experimental glaucoma. Invest. Ophthalmol. Vis. Sci. *53*, 3847–3857.

Kasahara, A., Cipolat, S., Chen, Y., Dorn, G.W., Scorrano, L., and Scorrano, L. (2013). Mitochondrial fusion directs cardiomyocyte differentiation via calcineurin and Notch signaling. Science (New York, N.Y.) *342*, 734–737.

Khacho, M., Harris, R., and Slack, R.S. (2019). Mitochondria as central regulators of neural stem cell fate and cognitive function. Nat. Rev. Neurosci. *20*, 34–48.

Kivlin, J.D., Lovrien, E.W., Bishop, D.T., and Maumenee, I.H. (1983). Linkage analysis in dominant optic atrophy. Am. J. Hum. Genet. *35*, 1190–1195.

Kjer, B., Eiberg, H., Kjer, P., and Rosenberg, T. (1996). Dominant optic atrophy mapped to chromosome 3q region 4. Acta Ophthalmol. Scand. *74*, 3–7.

Kruczek, K., and Swaroop, A. (2020). Pluripotent stem cell-derived retinal organoids for disease modeling and development of therapies. Stem Cell. *38*, 1206–1215.

Kuwahara, A., Ozone, C., Nakano, T., Saito, K., Eiraku, M., and Sasai, Y. (2015). Generation of a ciliary margin-like stem cell niche from self-organizing human retinal tissue. Nat. Commun. *6*, 6286.

Liu, S., Xiang, K., Yuan, F., and Xiang, M. (2023). Generation of self-organized autonomic ganglion organoids from fibroblasts. iScience *26*, 106241.

Lodi, R., Tonon, C., Valentino, M.L., Iotti, S., Clementi, V., Malucelli, E., Barboni, P., Longanesi, L., Schimpf, S., Wissinger, B., et al. (2004). Deficit of in vivo mitochondrial ATP production in OPA1-related dominant optic atrophy. Ann. Neurol. *56*, 719–723.

Nakano, T., Ando, S., Takata, N., Kawada, M., Muguruma, K., Sekiguchi, K., Saito, K., Yonemura, S., Eiraku, M., and Sasai, Y. (2012). Self-formation of optic cups and storable stratified neural retina from human ESCs. Cell Stem Cell *10*, 771–785.

Nestorowa, S., Hamey, F.K., Pijuan Sala, B., Diamanti, E., Shepherd, M., Laurenti, E., Wilson, N.K., Kent, D.G., and Göttgens, B. (2016). A single-cell resolution map of mouse hematopoietic stem and progenitor cell differentiation. Blood *128*, e20–e31.

Noguchi, M., and Kasahara, A. (2018). Mitochondrial dynamics coordinate cell differentiation. Biochem. Biophys. Res. Commun. *500*, 59–64.

O'Hara-Wright, M., and Gonzalez-Cordero, A. (2020). Retinal organoids: a window into human retinal development. Development *147*.

Olichon, A., Baricault, L., Gas, N., Guillou, E., Valette, A., Belenguer, P., and Lenaers, G. (2003). Loss of OPA1 perturbates the mitochondrial inner membrane structure and integrity, leading to cytochrome c release and apoptosis. J. Biol. Chem. *278*, 7743–7746.

Olichon, A., Landes, T., Arnauné-Pelloquin, L., Emorine, L.J., Mils, V., Guichet, A., Delettre, C., Hamel, C., Amati-Bonneau, P., Bonneau, D., et al. (2007). Effects of OPA1 mutations on mitochondrial morphology and apoptosis: relevance to ADOA pathogenesis. J. Cell. Physiol. *211*, 423–430.

Parfitt, D.A., Lane, A., Ramsden, C.M., Carr, A.-J.F., Munro, P.M., Jovanovic, K., Schwarz, N., Kanuga, N., Muthiah, M.N., Hull, S., et al. (2016). Identification and correction of mechanisms underlying inherited blindness in human iPSC-derived optic cups. Cell Stem Cell *18*, 769–781.

Sladen, P.E., Jovanovic, K., Guarascio, R., Ottaviani, D., Salsbury, G., Novoselova, T., Chapple, J.P., Yu-Wai-Man, P., and Cheetham, M.E. (2022). Modelling autosomal dominant optic atrophy associated with OPA1 variants in iPSC-derived retinal ganglion cells. Hum. Mol. Genet. *31*, 3478–3493.

Stroud, D.A., Surgenor, E.E., Formosa, L.E., Reljic, B., Frazier, A.E., Dibley, M.G., Osellame, L.D., Stait, T., Beilharz, T.H., Thorburn, D.R., et al. (2016). Accessory subunits are integral for assembly and function of human mitochondrial complex I. Nature *538*, 123–126.

Stuart, T., Butler, A., Hoffman, P., Hafemeister, C., Papalexi, E., Mauck, W.M., 3rd, Hao, Y., Stoeckius, M., Smibert, P., and Satija, R. (2019). Comprehensive integration of single-cell data. Cell *177*, 1888–1902.e21.

Sun, Y., and Ding, Q. (2017). Genome engineering of stem cell organoids for disease modeling. Protein Cell *8*, 315–327.

Tilokani, L., Nagashima, S., Paupe, V., and Prudent, J. (2018). Mitochondrial dynamics: overview of molecular mechanisms. Essays Biochem. *62*, 341–360.

VanderWall, K.B., Huang, K.C., Pan, Y., Lavekar, S.S., Fligor, C.M., Allsop, A.R., Lentsch, K.A., Dang, P., Zhang, C., Tseng, H.C., et al. (2020). Retinal ganglion cells with a glaucoma OPTN(E50K) mutation exhibit neurodegenerative phenotypes when derived from three-dimensional retinal organoids. Stem Cell Rep. *15*, 52–66.

Völkner, M., Zschätzsch, M., Rostovskaya, M., Overall, R.W., Busskamp, V., Anastassiadis, K., and Karl, M.O. (2016). Retinal organoids from pluripotent stem cells efficiently recapitulate retinogenesis. Stem Cell Rep. *6*, 525–538.

Weisschuh, N., Schimpf-Linzenbold, S., Mazzola, P., Kieninger, S., Xiao, T., Kellner, U., Neuhann, T., Kelbsch, C., Tonagel, F., Wilhelm, H., et al. (2021). Mutation spectrum of the OPA1 gene in a large cohort of patients with suspected dominant optic atrophy: Identification and classification of 48 novel variants. PLoS One *16*, e0253987.

Wu, F., Bard, J.E., Kann, J., Yergeau, D., Sapkota, D., Ge, Y., Hu, Z., Wang, J., Liu, T., and Mu, X. (2021). Single cell transcriptomics reveals lineage trajectory of retinal ganglion cells in wild-type and Atoh7-null retinas. Nat. Commun. *12*, 1465.

Xiang, M., Zhou, L., Peng, Y.W., Eddy, R.L., Shows, T.B., and Nathans, J. (1993). Brn-3b: a POU domain gene expressed in a subset of retinal ganglion cells. Neuron *11*, 689–701.

Xiao, D., Deng, Q., Guo, Y., Huang, X., Zou, M., Zhong, J., Rao, P., Xu, Z., Liu, Y., Hu, Y., et al. (2020). Generation of self-organized sensory ganglion organoids and retinal ganglion cells from fibroblasts. Sci. Adv. *6*, eaaz5858.

Yang, L., Tang, H., Lin, X., Wu, Y., Zeng, S., Pan, Y., Li, Y., Xiang, G., Lin, Y.F., Zhuang, S.M., et al. (2020). OPA1-exon4b binds to mtDNA D-loop for transcriptional and metabolic modulation, independent of mitochondrial fusion. Front. Cell Dev. Biol. *8*, 180.

Yu-Wai-Man, P., and Chinnery, P.F. (2013). Dominant optic atrophy: novel OPA1 mutations and revised prevalence estimates. Ophthalmology *120*, 1712–1712.e1.

Yu-Wai-Man, P., Griffiths, P.G., Burke, A., Sellar, P.W., Clarke, M.P., Gnanaraj, L., Ah-Kine, D., Hudson, G., Czermin, B., Taylor, R.W., et al. (2010). The prevalence and natural history of dominant optic atrophy due to OPA1 mutations. Ophthalmology *117*, 1538–1546.e1.

Yu-Wai-Man, P., Griffiths, P.G., and Chinnery, P.F. (2011). Mitochondrial optic neuropathies - disease mechanisms and therapeutic strategies. Prog. Retin. Eye Res. *30*, 81–114.

Zanna, C., Ghelli, A., Porcelli, A.M., Karbowski, M., Youle, R.J., Schimpf, S., Wissinger, B., Pinti, M., Cossarizza, A., Vidoni, S., et al. (2008). OPA1 mutations associated with dominant optic atrophy impair oxidative phosphorylation and mitochondrial fusion. Brain *131*, 352–367.

Zhang, H., Menzies, K.J., and Auwerx, J. (2018). The role of mitochondria in stem cell fate and aging. Development *145*, dev143420.

Zhang, Z., Xu, Z., Yuan, F., Jin, K., and Xiang, M. (2021). Retinal organoid technology: Where are we now? Int. J. Mol. Sci. *22*, 10244.

Zhou, W., Choi, M., Margineantu, D., Margaretha, L., Hesson, J., Cavanaugh, C., Blau, C.A., Horwitz, M.S., Hockenbery, D., Ware, C., and Ruohola-Baker, H. (2012). HIF1alpha induced switch from bivalent to exclusively glycolytic metabolism during ESC-to-EpiSC/hESC transition. EMBO J. *31*, 2103–2116.